Magnetism of Eu-doped GaN modulations by spinodal nanodecomposition

Akira Masago, Hikari Shinya, Tetsuya Fukushima, Kazunori Sato, and Hiroshi Katayama-Yoshida

Phys. Rev. B **98**, 214426 — Published 14 December 2018

DOI: 10.1103/PhysRevB.98.214426

Magnetism of Eu-doped GaN modulations by spinodal nanodecomposition

Akira Masago

Center for Spintronics Research Network,

Graduate School of Engineering Science,

Osaka University, 1-3 Machikaneyama,

*Toyonaka, Osaka 560-8531, Japan**

Hikari Shinya

Department of Engineering, Yokohama National University,

79-5 Tokiwadai, Hodogaya-ku, Yokohama, Kanagawa 240-8501, Japan and

Center for Spintronics Research Network,

Graduate School of Engineering Science,

Osaka University, 1-3 Machikaneyama,

*Toyonaka, Osaka 560-8531, Japan**

Tetsuya Fukushima

Institute for NanoScience Design, Osaka University,

1-3 Machikaneyama, Toyonaka, Osaka 560-5531, Japan and

Center for Spintronics Research Network,

Graduate School of Engineering Science,

Osaka University, 1-3 Machikaneyama,

*Toyonaka, Osaka 560-8531, Japan**

Kazunori Sato

Graduate School of Engineering, Osaka University,

2-1 Yamadaoka, Suita, Osaka, 565-0871, Japan and

Center for Spintronics Research Network,

Graduate School of Engineering Science,

Osaka University, Toyonaka, Osaka 560-8531, Japan

Hiroshi Katayama-Yoshida

Center for Spintronics Research Network, The University of Tokyo,

7-3-1 Hongo Bunkyo-ku, Tokyo 113-8656, Japan

Abstract

By the Monte-Carlo method, magnetic properties have been investigated for Eu-doped GaN involving internal nanostructures induced by nanoscale spinodal decomposition, where these nanostructures are spontaneously or artificially formed. In the present simulations, hysteretic and non-hysteretic magnetization curves are observed in the systems with the large-sized and small-sized nanostructures, respectively. These nanostructures affect the blocking temperatures as well. Furthermore, they influence temperature-dependent energy barriers of spin flipping; therefore, the simulations suggest that the magnetization is thermally stable. However, we observe that the blocking temperatures are smaller than the experimental values, which may be due to atomic vacancies.

PACS numbers:

I. INTRODUCTION

Eu-doped GaN is renowned for red light emitting diodes (LEDs);[1–5] whereas, it is interesting as a magnetic material.[6–10] Hashimoto et al. reported the magnetization effects in Eu-doped GaN showing a ferromagnetic hysteresis having constant magnetization with increasing temperature,[8] depending on the external field; it was concluded that such a condition was induced either by ferromagnetism or superparamagnetism via the Ruderman-Kittel-Kasuya-Yosida (RKKY) interaction.[8,11–13] Nunokawa et al. reported non-hysteretic sigmoidal curves for Eu-doped GaN and its derivatives.[9]

From a theoretical viewpoint, Said et al., Svane et al., Cruz et al., and our group reported the investigation of electronic structures by ab-initio calculations.[14–17] Both the research groups of Said and Svane have suggested that Eu-doped zincblende GaN involves the localized Eu 4f-states in the band gap; however, Said et al. reported that it is ferromagnetic, whereas Svane et al. reported that it is antiferromagnetic.[14,15] Both our and Cruz's groups investigated the Eu-doped wurtzite GaN including codopants using the Vienna Ab-initio Simulation Package (VASP) code,[4,16] and have suggested that the localized 4f-states of Eu are localized at the band edges and that the ferromagnetic states are stable.

Meanwhile, Lu et al. reported that ErGaSb, which is a similar compound to Eu-doped GaN, exhibits nanometer-scaled density modulations that are induced by spinodal decomposition.[18,19] Herein, we refer to these structures as *internal nanostructures*. InGaN and some rare-earth doped materials also exhibits spinodal decomposition and form various crystalline internal nanostructures,[20–23] among which most are strongly dependent on the annealing temperature and impurity concentration.

In our previous study, we depicted that the calculated mixing energy versus composition profile in Eu-doped GaN formed a convex upward arc; therefore, it is expected that Eu-doped GaN can also form nanostructures induced by spinodal decomposition. The chemical pair interaction, which was calculated using the generalized perturbation method,[24] also indicated an attractive trend between Eu ions in the zincblende GaN matrix.[25–28] Using this chemical pair interaction, we obtained internal nanostructures or internal clusters of EuN depending on the annealing temperature, number of annealing steps, and Eu ion concentration.[25] We proposed two phases that are called *Dairiseki* and *Konbu* phases. The former phase occurs spontaneously and involves nano-dots, whereas the latter phase is artificially generated as

to have nano-rods.[27,28]

Figures 1, 2, and 3 exhibit typical phases proposed in our previous papers. Figure 1 depicts a homogeneous distribution of Eu ions that is generated randomly in the calculation cell (a 20×20×20 supercell), where particles indicate Eu ions located at Ga-sites on the FCC lattice points, and Ga and N ions are omitted. Figure 2 depicts the Dairiseki and the Konbu phases that are generated by Monte-Carlo simulations with 10,000 annealing steps, where the scaled temperature of $k_{\rm B}T/|V_{01}|$ was set to 0.5, which corresponds to 428 K, and V_{01} indicates the chemical pair interaction between the nearest neighbor pair of Eu ions.[25] Figure 3 depicts these phases that are generated with 1,000,000 annealing steps under the temperature of 0.5. The Dairiseki phase can be generated using a crystal growth method: the three dimensional diffusion of impurities or dopants is allowed. The Konbu phase can be generated by a method: the two dimensional diffusion is allowed on each surface of the layer-by-layer crystal growth.

Although conventional top-down processing methods, such as photolithography, are typically used for microfabrication of such internal nanostructures, bottom-up processing can be achieved via spinodal decomposition. The Dairiseki and Konbu phases could be used for the microfabrication of nanostructures for circularly polarized luminescence, solid semiconducting laser, and qubits of quantum computing applications. In this study, we simulated magnetization as a function of external magnetic field for the internal nanostructures that are introduced in our previous study.[25] These values of magnetization are discussed with respect to the blocking temperatures.

II. METHODS

The ab-initio calculations use the Korringa-Kohn-Rostoker (KKR) method with a coherent potential approximation (CPA) in the Akai-KKR package.[29–32] CPA, in which the multiple scattering effect is replaced by an effective-medium potential,[33,34] treats the randomness of the doped impurities in the host semiconductors. Therefore, supercells are not usually used in CPA. The KKR method has been validated by Svane et al. for GaAs and GaN in the presence of rare-earth impurities.[15] All the spin-polarization and the semi-relativistic calculations that were performed in this study included the spin-orbit interaction, where the Eu 4f-states were considered to be the valence states. The exchange energy is parameterized

via the Moruzzi-Janak-Williams (MJW) formula and the self-interaction correction in the local density approximation (SIC-LDA).[35] The number of k-sampling points was 1,000.

We calculated the interaction J_{ij} between Eu impurities in GaN for quantitatively evaluating the magnetic properties within Liechtenstein's formula.[36] This approach considers a perturbation due to an infinitesimal rotation of the magnetic moments of two Eu atoms in the CPA medium. The energy change due to the perturbation is calculated in accordance with the magnetic force theorem and it is mapped onto the classical Heisenberg model.[37,38] J_{ij} is provided by

$$J_{ij} = \frac{1}{4\pi}\mathrm{Im}\int_{E_\mathrm{B}}^{E_\mathrm{F}} dE\ \mathrm{Tr}_L\left\{\Delta_i T_\uparrow^{ij}\Delta_j T_\downarrow^{ji}\right\}, \tag{1}$$

where $\Delta_i = t_{i\uparrow}^{-1} - t_{i\downarrow}^{-1}$ is the difference in the atomic t-matrix between the spin-up and spin-down states. $T_{\uparrow(\downarrow)}^{ij}$ is the off-diagonal scattering path operator between sites i and j for the spin-up (down) state. Tr_L is the trace over the orbital variables, ℓ and m. The energy integration is performed from the bottom of the valence band, E_B, to the Fermi energy, E_F.

A general form of the Hamiltonian of the Heisenberg model is provided by

$$H = -\sum_i \sum_j \boldsymbol{S}_i \cdot \mathcal{J}_{ij}\boldsymbol{S}_j, \tag{2}$$

where the sums run over all atoms in the crystal, $\boldsymbol{S}_i$ is a classical vector of dimension 3, which represents a spin at lattice site i, and $\mathcal{J}_{ij}$ is a 3×3 matrix. Udvardi et al. reported that $\mathcal{J}$ has to be decomposed as an isotropic, anti-symmetric, and a traceless symmetric part:

$$\mathcal{J}_{ij} = J_{ij}\mathcal{I} + \mathcal{J}_{ij}^A + \mathcal{J}_{ij}^S, \tag{3}$$

where $\mathcal{I}$ is the identity tensor, and the anti-symmetric part is related to the Dzyaloshinskii-Moriya vector.[39] In our simulations, the calculated J_{ij} includes small fluctuations (1.02 - 1.33 mRy) at the first nearest neighbor pair of Eu ions. We regarded it as numerical errors, and averaged these values every ij.

In our simulations of the magnetization as functions of temperature and external magnetic field, a scalar Heisenberg model is provided by

$$H = -\sum_{i\neq j} J_{ij}\boldsymbol{e}_i \cdot \boldsymbol{e}_j - \sum_i K(e_i^z)^2 - \mu B^z \sum_i e_i^z, \tag{4}$$

where the sums run over all atomic pairs in the crystal, J_{ij} is given by Eq. (1), $\boldsymbol{e}_i$ is the unit vector parallel to the magnetization at site i, B^z is the external field along the z-axis, and

μ is the absolute value of the magnetic moment. $K(e_i^z)$ is the magnetic anisotropy term, which was very small value (0.001) in order to assist computational stability of the Monte-Carlo simulations, especially in the homogeneous phase. We think it is acceptable in this study, because Eu ions, which become divalent and trivalent ions in GaN, have half-filling and total moment $J = 0$, respectively. Therefore, it is guessed that the magnetic anisotropy about Eu in GaN depends on more strongly on the impurity clusters and atomic vacancies than the single-ion magnetic anisotropy. In order to describe meta-stable states that are responsible for the magnetic hysteresis, the local algorithm method introduced by Dimitrov was used.[40,41] In the local algorithm, a trial state is chosen of states near the current position in the phase space; whereas, the trial state is randomly selected in the Metropolis algorithm in the Monte Carlo method. The temperature and the external field were scaled by $k_{\mathrm{B}}T/|J_{01}|$ and $|J_{01}|$, respectively, and the magnetization was normalized so as to become 1 when all spins were parallel to the external field. The calculation cell was a $20 \times 20 \times 20$ zincblende sublattice. The number of the Monte-Carlo steps was 36,000 every external field value.

For simulating of the Curie temperature, we used the cumulant intersection method proposed by Binder to determine the critical point,[42] i.e. the Curie temperature is estimated from the intersection of the fourth order cumulants,[40,41]

$$U_L(T) = 1 - \frac{\langle M^4 \rangle}{3\langle M^2 \rangle^2} \tag{5}$$

with different lattice size, L, where M is the magnetization. Here, three different lattice sizes, $(L \times L \times L) = (14 \times 14 \times 14), (18 \times 18 \times 18)$, and $(22 \times 22 \times 22)$ were used. In the cumulant calculations, the Eu configuration was not annealed, i.e., the homogenous Eu distribution was considered here. For taking average of the Eu configuration, we prepared 16 different random configurations of the Eu sites, Then, 62,000 Monte Carlo steps were performed for each temperature. We discarded first 2,000 Monte Carlo steps to obtain thermal equilibrium states. The system magnetization was averaged over 3,000 spin configurations every 20 Monte Carlo steps.

The blocking temperature, T_{B}, was estimated by Sato's formula.[41] A spin configuration in which all spins are aligned anti-parallel to the external field keeps meta-stable for low temperatures due to the energy barrier originated from the weak external field (and the magnetic anisotropy), but the magnetization of the anti-parallel configuration suddenly reverses once thermal fluctuation becomes larger enough to overcome the energy barrier. When

the magnetization reaches the maximum after reverse, we defined the temperature as the blocking temperature.

III. RESULTS

Figure 4 depicts the magnetic pair interaction between Eu ions in the zincblende GaN matrix as a function of the inter-ionic distance. The interaction was normalized by the nearest neighboring pair, and positive and negative values indicated the ferromagnetic and antiferromagnetic interactions, respectively. The magnetic pair interaction values for Eu concentrations of 6%, 7%, 8%, 9%, 10%, 11%, and 12% are depicted in Fig. 4, and the magnetization for each samples exhibits short-range ferromagnetism, similar to that observed in the double exchange interaction (rather than the RKKY interaction).

Figure 5 depicts the cumulants as a function of temperature, T. They are plotted for the three supercell sizes, (14×14×14), (18×18×18), and (22×22×22). It is only of the homogeneous distribution of Eu ions (10%) due to calculation costs. It indicates that the Curie temperature is approximately between 0.12 and 0.14.

We estimated the blocking temperatures of homogeneous (Fig. 1), Dairiseki (Fig. 3(a)), and Konbu phases (Fig. 3(b)), where the two phases have virtually maximum sizes of the internal nanostructures. Figure 6 depicts the simulated magnetization of the three phases under a small external magnetic field with increasing temperature. The blocking temperature of the homogeneous phase is approximately 50×10^{-3}, whereas it is slightly higher in the Dairiseki phase. The magnetization in the Konbu phase exhibits multiple steps and a higher blocking temperature of approximately 150×10^{-3}. This is because the clusters in the Konbu phase is larger than those in the Dairiseki phase. In the Konbu phase, the number of magnetic impurities magnetically connecting to other magnetic impurities are larger than the other phases, and the clusters form a variety of shapes: non-uniform diameter, termination in the middle, and branches. Contrary, in the Dairiseki phase, the number of magnetic impurities are small, and the clusters form quantum dots with similar shapes and sizes. Therefore, the Konbu phase has a higher energy barrier and more persistent initial states as compared to those observed in other phases. Moreover, the energy barrier affects the thermal decay of magnetization. The magnetizations of the Dairiseki and Konbu phase decay slowly, whereas that of the homogeneous phase decays quickly. We guess that such

internal nanostructures cause the thermally stable magnetization that is observed in the study conducted by Hashimoto.[8]

Figure 7 denotes the magnetization versus external field at a temperature of 1.0, which is significantly higher than the blocking temperature. The homogeneous phase exhibits a nonmagnetic behavior. At this temperature, the thermal fluctuations are large, and the local magnetic moments freely flip between the two alignments regardless of the barrier. The Dairiseki phase exhibits a paramagnetic behavior, because magnetic moments can move to the stable state over the barrier due to thermal fluctuation, but they hardly go back to the meta-stable state. According to statistical thermodynamics, some meta-stable spin states can persist, and the population difference between the two states contributes to magnetization. The Konbu phase exhibits paramagnetism, similar to that observed in the Dairiseki phase; however, the larger number of interconnected spins result in a larger energy barrier and magnetic susceptibility and saturation magnetization values in the Konbu phase as compared with those observed in the Dairiseki phase.

Figure 8 denotes the magnetization versus external magnetic field at a temperature of 0.01, which is lower than the blocking temperature. Every phase exhibits a hysteresis curve that is indicative of superparamagnetism. Because thermal fluctuation is small at this temperature, a given spin requires a large external field change state due to the local magnetic pair interactions. Since the number of magnetic impurities per nanostructure is proportional to the energy barrier height, the Konbu phase exhibits the largest hysteresis of the three phases.

As described above, in systems with large clusters at high and low temperatures compared with the blocking temperatures, the properties are clear. Next, we consider the properties in indecisive systems, which have small clusters and a temperature comparable to the blocking temperatures. Figure 9 depicts the simulated magnetization of the three phases (Figs. 1-2) with increasing temperature, where the line of the homogeneous phase is the same as one in Fig. 6. Herein, the Dairiseki and Konbu phases were generated by the annealing steps of 10,000 under the same temperature (0.5) and same cell sizes as above. The blocking temperatures of the Dairiseki and Konbu phases become lower than those by the annealing steps of 1M. This is because the cluster sizes of the two phases are smaller. However, it seems to be strange that the blocking temperature of the Dairiseki phase becomes lower than that of the homogeneous phase.

Figure 10 exhibits a plot of magnetization versus external field at a temperature of 0.1, which is comparable to the blocking temperature. The Magnetization curve of the Dairiseki phase is non-hysteretic, whereas those of the homogeneous and the Konbu exhibit show small and large hysteresis, respectively. If only the internal nanostructures were a cause of the hysteresis, the magnetization curves of the Dairiseki and homogeneous phases should exhibit hysteretic and non-hysteretic, respectively.

This is because the relation between the interstitial length among the magnetic clusters and the effective length of the magnetic pair interaction. The magnetic pair interaction comprises the short-, middle-, and long-range components as shown in Fig. 4. The short-range component is intense, and the long-range component is essentially zero (accurately, the interactions, J_{ij}, over the 12th nearest neighbor were considered to be zero in the simulations). The middle-range component is small but non-zero as depicted in Fig. 4. Therefore, the middle-range component weakly couples spins in the homogeneous phase. However, the middle-range component does not couple spins between different clusters in the Dairiseki and Konbu phases, because no spin areas lie among the clusters. In the two phases, only the short-range component, which works within each cluster, distributes the magnetization. In particular, in the Dairiseki phase, the number of spins in each cluster is so small in this condition that the hysteresis does not appear.

The above discussion suggests the a trend that the magnetization turns from decrease to increase with nanostructure growing. This is because annealing grows not only EuN clusters but also GaN clusters, which are non-spin areas; therefore, the Eu ions that coupled each other before annealing by the middle-ranged magnetic pair interaction are separated between the EuN clusters. As a result, the magnetization decreases once. As the annealing proceeds more, the number of spins in a single EuN cluster increases. The magnetization turns to increase finally.

As depicted in Fig. 6, the blocking temperatures of the homogeneous, Dairiseki, and Konbu phases are 0.06, 0.08, and 0.15, respectively. Using $k_{\mathrm{B}}T_{\mathrm{B}}/|J_{01}|$, these values are converted to 23.2 K, 30.9 K, and 57.9 K, where $J_{01} = 0.00122$. Herein, we note that the difference of summation methods between the general and scalar Heisenberg Hamiltonians, Eq.(2) and Eq.(4). The former sums run over all atoms and the latter does over all pairs; therefore, J_{ij} in Eq. (4) has a factor of 2 smaller than it in Eq. (1) and Fig. 4. Hashimoto et al. reported a finite magnetic moment at room temperature, as well as a significant decrease

in magnetization from 5 K to 70 K and a slow decrease in magnetization from 100 K to 300 K.[8] Our simulated blocking temperature is smaller than their experimental value, though the crystal structures are different from each other. In Gd-doped GaN, colossal magnetic moments and the ferromagnetism at a temperature above the room temperature have been reported.[43,44] Gohda and Oshiyama proposed that Ga vacancies induce the colossal magnetic moments per Gd atom.[45] Furthermore, Thiess et al. proposed that the Ga vacancies provide significantly strong and robust ferromagnetic interactions between spins that are localized on the nitrogen near the vacancies.[46,47] Eu-doped GaN may also be affected by such native defects like Ga vacancies. We will focus on such effect in future studies. If deep-impurity-bands are populated in such materials, robust ferromagnetic interactions may be realized via Zener's double exchange interactions, which are generated by partial occupation of highly correlated deep-impurity bands[48–50]

IV. SUMMARY

Monte-Carlo simulations of magnetization under external magnetic fields were performed on Eu-doped GaN zincblende crystalline nanostructures formed by spinodal decomposition. The magnetization curves depict hysteresis at temperatures lower than the simulated blocking temperature and non-hysteresis at a temperature higher than the blocking temperature. The difference is induced by competition among the thermal fluctuation, the energy barriers of spin flipping, and the internal cluster sizes. The small thermal dependence of the blocking temperature, which is observed in experiments, is reproduced by the simulations in this study. This is based on the larger energy barriers with larger internal EuN clusters. However, the simulated blocking temperature is smaller than the experimental one. It may be due to atomic vacancies in GaN.

Acknowledgements

This work was partly supported by JST CREST (JPMJCR1777). This work was partly supported by JSPS KAKENHI Grant Numbers A242260090, 16K21155, and 18K04926. This work was partly supported by Advanced Low Carbon Technology Research and Development Program (ALCA), "High-efficiency Energy Conversion by Spinodal Nano-decomposition" of

Japan Science and Technology Agency (JST), and by Japan Society for the Promotion of Science. This work was partly supported by JSPS Core-to-Core Program (A) Advanced Research Networks "Computational Nano-materials Design on Green Energy". The computation in this work was done using the facilities of the Supercomputer Center, the Institute for Solid State Physics, the University of Tokyo. T.F. thanks the supports from "Building of Consortia for the Development of Human Resources in Science and Technology".

---

* Electronic address: masago@mp.es.osaka-u.ac.jp

[1] S. Morishima, T. Maruyama, M. Tanaka, Y. Masumoto, and K. Akimoto, Phys. Status Solidi A **176**, 113 (1999).

[2] J. Heikenfeld, M. Garter, D. S. Lee, R. Birkhahn, and A. J. Steckl, Appl. Phys. Lett. **75**, 1189 (1999).

[3] A. Nishikawa, T. Kawasaki, N. Furukawa, Y. Terai, and Y. Fujiwara, Appl. Phys. Express **2**, 071004 (2009).

[4] A. Masago, T. Fukushima, K. Sato, and H. Katayama-Yoshida, Appl. Phys. Express **7**, 071005 (2014).

[5] A. Masago, T. Fukushima, K. Sato, and H. Katayama-Yoshida, Appl. Phys. Express **7**, 121002 (2014).

[6] Y. Li, S. Yu, X. Meng, Y. Liu, Y. Zhao, F. q. Liu, and Z. Wang, J. Phys. D **46**, 215101 (2013).

[7] H. Asahi, Y. K. Zhou, M. Hashimoto, M. S. Kim, X. J. Li, S. Emura, and S. Hasegawa, J. Phys.: Condens. Matter **16**, S5555 (2004).

[8] M. Hashimoto, A. Yanase, R. Asano, H. Tanaka, H. Bang, K. Akimoto, and H. Asahi, Jpn. J. Appl. Phys. **42**, L1112 (2003).

[9] T. Nunokawa, A. Koizumi, T. Sakurai, M. Matsuda, W. Zhu, H. Ohta, and Y. Fujiwara, in *MRS Fall Meeting* (Boston, USA, 2016), p. En.2.5.06.

[10] K. Sato, J. Kudrnovský, P. H. Dederichs, O. Eriksson, I. Turek, B. Sanyal, G. Bouzerar, H. Katayama-Yoshida, V. A. Dinh, T. Fukushima, et al., Rev. Mod. Phys. **82**, 1633 (2010).

[11] M. A. Ruderman and C. Kittel, Phys. Rev. **96**, 99 (1954).

[12] T. Kasuya, Progr. Theoret. **16**, 45 (1956).

[13] K. Yosida, Phys. Rev. **106**, 893 (1957).

[14] S. Goumri-Said and M. B. Kanoun, J. Phys. D **41**, 035004 (2008).

[15] A. Svane, N. E. Christensen, L. Petit, Z. Szotek, and W. M. Temmerman, Phys. Rev. B **74**, 165204 (2006).

[16] A. V. BrunoCruz, P. P. Shinde, V. Kumar, and J. M. Zavada, Phys. Rev. B **85**, 045203 (2012).

[17] A. Masago, T. Fukushima, K. Sato, and H. Katayama-Yoshida, Jpn. J. Appl. Phys. **53**, 061001 (2014).

[18] H. Lu, D. G. Ouellette, S. Preu, J. D. Watts, B. Zaks, P. G. Burke, M. S. Sherwin, and A. C. Gossard, Nano Lett. **14**, 1107 (2014).

[19] J. K. Kawasaki, B. D. Schultz, H. Lu, A. C. Gossard, and C. J. Palmstrom, Nano Lett. **13**, 2895 (2013).

[20] C. Tessarek, S. Figge, T. Aschenbrenner, S. Bley, A. Rosenauer, M. Seyfried, J. Kalden, K. Sebald, J. Gutowski, and D. Hommel, Phys. Rev. B **83**, 115316 (2011).

[21] S. Figge, C. Tessarek, T. Aschenbrenner, and D. Hommel, physica status solidi b **248**, 1765 (2011).

[22] R. Salas, S. Guchhait, S. D. Sifferman, K. M. McNicholas, V. D. Dasika, E. M. Krivoy, D. Jung, M. L. Lee, and S. R. Bank, Appl. Phys. Lett. **106**, 081103 (2015).

[23] L. E. Clinger, G. Pernot, T. E. Buehl, P. G. Burke, A. C. Gossard, C. J. Palmstrom, A. Shakouri, and J. M. O. Zide, J. Appl. Phys. **111**, 094312 (2012).

[24] F. Ducastelle and F. Gautier, J. Phys. F **6**, 2039 (1976).

[25] A. Masago, T. Fukushima, K. Sato, and H. Katayama-Yoshida, Jpn. J. Appl. Phys. **55**, 070302 (2016).

[26] T. Dietl, K. Sato, T. Fukushima, A. Bonanni, M. Jamet, A. Barski, S. Kuroda, M. Tanaka, P. N. Hai, and H. Katayama-Yoshida, Rev. Mod. Phys. **87**, 1311 (2015).

[27] K. Sato, H. Katayama-Yoshida, and P. H. Dederichs, Jpn. J. Appl. Phys. **44**, L948 (2005).

[28] T. Fukushima, K. Sato, H. Katayama-Yoshida, and P. H. Dederichs, Jpn. J. Appl. Phys. **45**, L416 (2006).

[29] J. Korringa, Physica **13**, 392 (1947).

[30] W. Kohn and N. Rostoker, Phys. Rev. **94**, 1111 (1954).

[31] G. M. Stocks, W. M. Temmerman, and B. L. Gyorffy, Phys. Rev. Lett. **41**, 339 (1978).

[32] H. Akai, J. Phys. Soc. Jpn **51**, 468 (1982).

[33] H. Shiba, Prog. Theor. Phys. **46**, 77 (1971).

[34] P. Soven, Phys. Rev. B **2**, 4715 (1970).

[35] M. Toyoda, H. Akai, K. Sato, and H. Katayama-Yoshida, Physica B **376-377**, 647 (2006).

[36] A. I. Liechtenstein, M. I. Katsnelson, V. P. Antropov, and V. A. Gubanov, J. Magn. Magn. Mater. **67**, 65 (1987).

[37] A. Oswald, R. Zeller, P. J. Braspenning, and P. H. Dederichs, J. Phys. F: Met. Phys. **15**, 193 (1985).

[38] A. R. Machintosh and O. K. Andersen, *Electrons at the Fermi surface* (Cambridge Univ Press, London, 1980).

[39] L. Udvardi, L. Szunyogh, K. Palotas, and P. Weinberger, Phys. Rev. B **68**, 104436 (2003).

[40] D. A. Dimitrov and G. M. Wysin, Phys. Rev. B **54**, 9237 (1996).

[41] K. Sato, T. Fukushima, and H. Katayama-Yoshida, Jpn. J. Appl. Phys. **46**, L682 (2007).

[42] K. Binder, Z. Phys. B: Condensed Matter **43**, 119 (1981).

[43] S. Dhar, O. Brandt, M. Ramsteiner, V. F. Sapega, and K. H. Ploog, Phys. Rev. Lett. **94**, 037205 (2005).

[44] S. Dhar, L. Perez, O. Brandt, A. Trampert, K. H. Ploog, J. Keller, and B. Beschoten, Phys. Rev. B **72**, 245203 (2005).

[45] Y. Gohda and A. Oshiyama, Phys. Rev. B **78**, 161201(R) (2008).

[46] A. Thiess, P. H. Dederichs, R. Zeller, S. Blugel, and W. R. L. Lambrecht, Phys. Rev. B **86**, 180401(R) (2012).

[47] A. Thiess, S. Blugel, P. H. Dederichs, R. Zeller, and W. R. L. Lambrecht, Phys. Rev. B **92**, 104418 (2015).

[48] K. Kenmochi, M. Seike, K. Sato, A. Yanase, and H. Katayama-Yoshida, Jpn J. Appl. Phys. **43**, L934 (2004).

[49] M. Seike, K. Sato, and H. Katayama-Yoshida, Jpn. J. Appl. Phys. **50**, 090204 (2011).

[50] M. Seike, V. A. Dinh, T. Fukushima, K. Sato, and H. Katayama-Yoshida, Jpn. J. Appl. Phys. **51**, 050201 (2012).

[51] K. Momma and F. Izumi, J. Appl. Crystallogr. **44**, 1272 (2011).

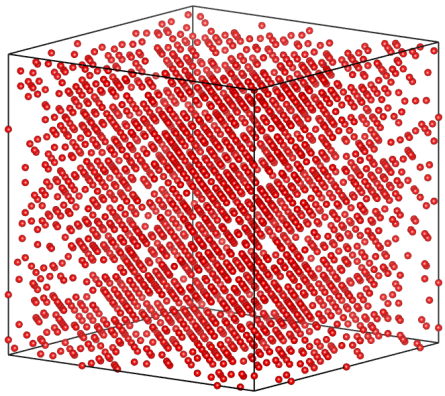

FIG. 1: (Color online) Atomic configuration of the homogeneous phase. The cube indicates a calculation cell, which is a 20×20×20 FCC supercell with a single side of 93.4 Å. A periodic boundary condition was applied along the lateral axes. The supercell contains 32,000 particles (Eu, Ga, and N ions) on a zincblende type matrix of which 10% are Eu ions, occupying the Ga-sites. Every particle is a single Eu ion; Ga and N ions are omitted. Figures of atomic configurations were prepared using VESTA, visualization for electronic and structural analysis.[51]

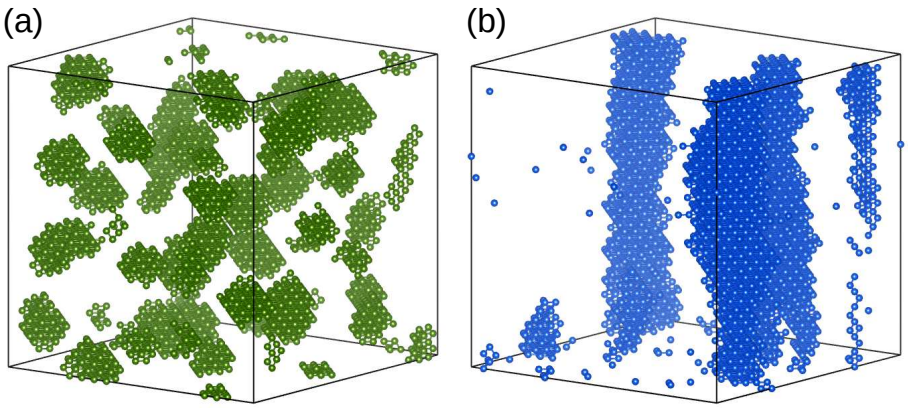

FIG. 2: (Color online) Atomic configuration of the Dairiseki (a) and Konbu phases (b) after 10,000 Monte-Carlo annealing steps. In the Konbu phase simulation, the crystal grows from the bottom upwards along the vertical direction. A concentration of 10% Eu ions is used for both phases. In the Dairiseki phase, the supercell contains 12 clusters of 100 or more Eu ions among which the maximum cluster contains 254 Eu ions. In the Konbu phase, the supercell contains 3 clusters of 100 or more Eu ions among which the maximum cluster contains 1,045 Eu ions.

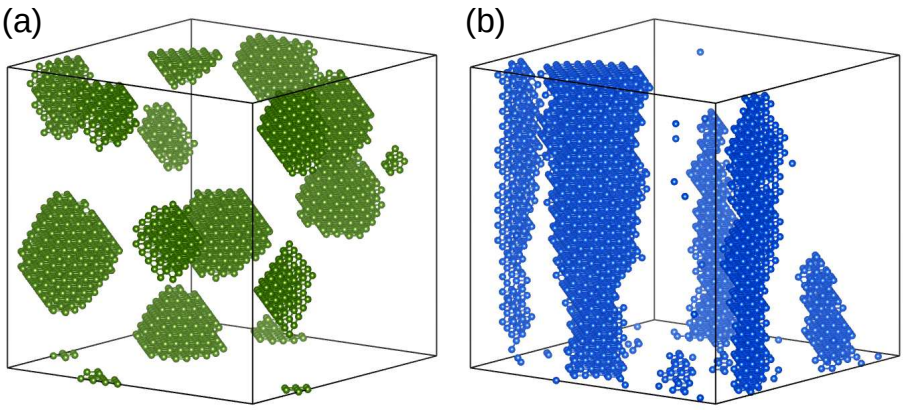

FIG. 3: (Color online) Atomic configuration of the Dairiseki (a) and Konbu phases (b) after 1,000,000 Monte-Carlo annealing steps. A concentration of 10% Eu ions is used. In the Dairiseki phase, the supercell contains 8 clusters of 100 or more Eu ions among which the maximum cluster contains 654 Eu ions. In the Konbu phase, the supercell contains 4 clusters of 100 or more Eu ions among which the maximum cluster contains 1,862 Eu ions. A periodic boundary condition was applied along the lateral axes; therefore, single nanorods across the cell boundary appear as separated rods in the Konbu phase.

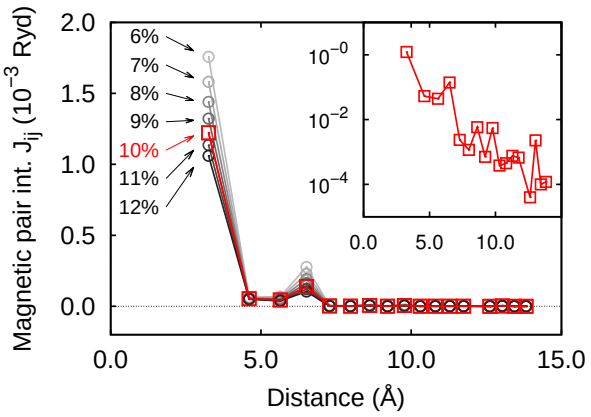

FIG. 4: (Color online) The magnetic pair interaction J_{ij} between the Eu ions in the zincblende GaN matrix. Numerical values (%) denote the concentration of the Eu ion. The concentration of Eu ranges from 6% to 12% in steps of 1%. J_{ij} was used at a concentration of 10% (red boxes) to perform the magnetization simulations. (inset) J_{ij} with a concentration of 10% on a logarithm scale.

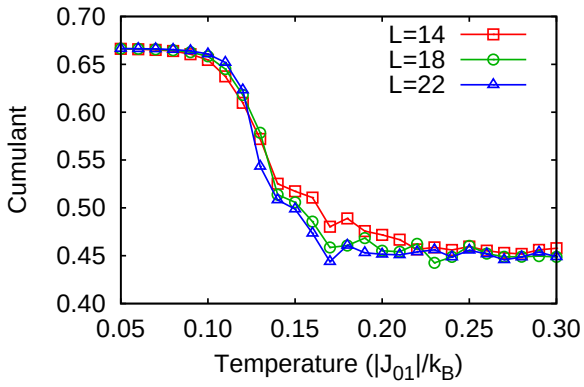

FIG. 5: (Color online) The cumulant $U_L(T)$ intersection plots in the homogeneous phase. T_C was calculated from the intersection of the 4th order cumulant for three supercell sizes (14×14×14), (18×18×18), and (22×22×22), which are indicated by red boxes, green circles, and blue triangles.

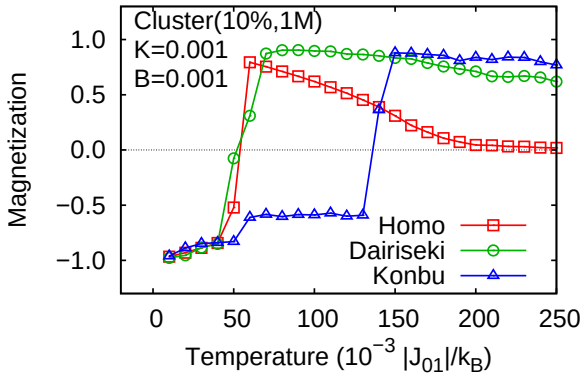

FIG. 6: (Color online) Magnetization as a function of temperature for homogeneous, Dairiseki (concentration=10%, annealing step=1,000,000), and Konbu (concentration=10%, annealing step=1,000,000) phases, demonstrating the blocking temperature. The magnetization is normalized so as to become 1 when all spins are parallel. The anisotropic constant K is 0.001, and the external field is 0.001.

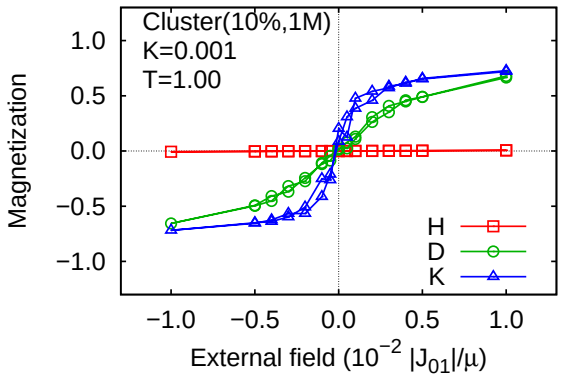

FIG. 7: (Color online) Magnetization versus external field at a high temperature. The magnetization is normalized so as to become 1 when all spins are parallel. The anisotropy constant K is 0.001, and temperature is 1.0. Red boxes, green circles, and blue triangles indicate the magnetization of the homogeneous, Dairiseki, and Konbu phases, respectively.

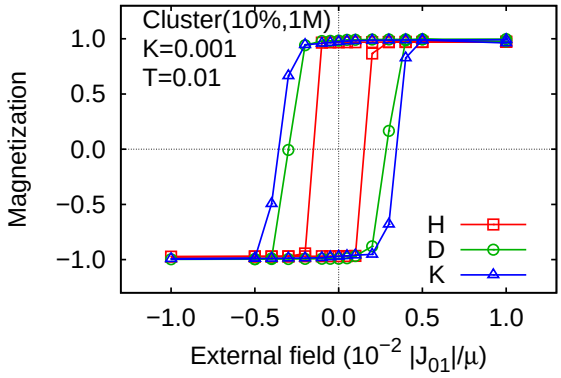

FIG. 8: (Color online) Magnetization versus external field at a low temperature. The anisotropy constant K is 0.001, and temperature is 0.01. Red boxes, green circles, and blue triangles indicate the magnetization of the homogeneous, Dairiseki, and Konbu phases, respectively.

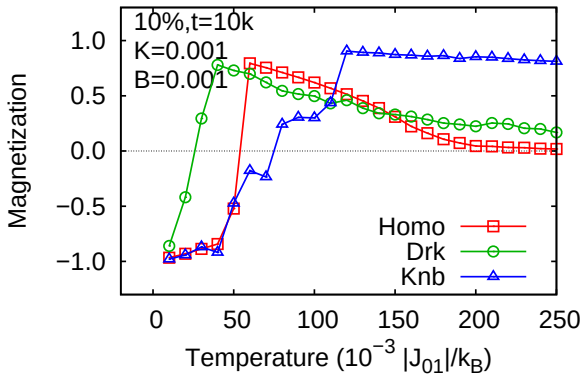

FIG. 9: (Color online) Magnetization as a function of temperature for homogeneous, Dairiseki (concentration=10%, annealing step=1,0,000), and Konbu (concentration=10%, annealing step=1,0,000) phases, demonstrating the blocking temperature. The magnetization is normalized so as to become 1 when all spins are parallel. The anisotropic constant K is 0.001, and the external field is 0.001.

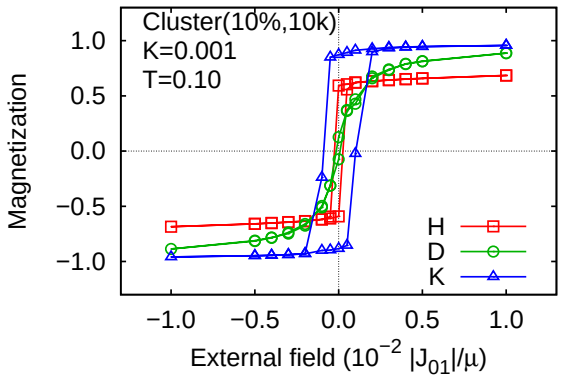

FIG. 10: (Color online) Magnetization versus external field near the blocking temperature. The anisotropy constant K is 0.001, and temperature is 0.1. Red boxes, green circles, and blue triangles indicate the magnetization of the homogeneous, Dairiseki, and Konbu phases, respectively. The nanostructures were generated with 1,000 annealing steps.